AGU PUBLICATIONS

Water Resources Research

RESEARCH ARTICLE
10.1002/2016WR018884

Rock fracture grouting with microbially induced carbonate precipitation

James M. Minto[1], Erica MacLachlan[1], Gráinne El Mountassir[1], and Rebecca J. Lunn[1]

[1]Department of Civil and Environmental Engineering, University of Strathclyde, Glasgow, UK

Key Points:
- Effectiveness of microbially induced carbonate precipitation for sealing artificial rock fractures shown
- Relationship between precipitated $CaCO_3$ and change in flow paths visible. Precipitation was controllable
- Three orders of magnitude reduction in fracture transmissivity achieved with three injection cycles over 3 days

Correspondence to:
J. M. Minto,
james.minto@strath.ac.uk

Citation:
Minto, J. M., E. MacLachlan, G. El Mountassir, and R. J. Lunn (2016), Rock fracture grouting with microbially induced carbonate precipitation, *Water Resour. Res.*, *52*, doi:10.1002/2016WR018884.

Received 3 MAR 2016
Accepted 30 OCT 2016
Accepted article online 3 NOV 2016

Abstract Microbially induced carbonate precipitation has been proposed for soil stabilization, soil strengthening, and permeability reduction as an alternative to traditional cement and chemical grouts. In this paper, we evaluate the grouting of fine aperture rock fractures with calcium carbonate, precipitated through urea hydrolysis, by the bacteria *Sporosarcina pasteurii*. Calcium carbonate was precipitated within a small-scale and a near field-scale (3.1 m^2) artificial fracture consisting of a rough rock lower surfaces and clear polycarbonate upper surfaces. The spatial distribution of the calcium carbonate precipitation was imaged using time-lapse photography and the influence on flow pathways revealed from tracer transport imaging. In the large-scale experiment, hydraulic aperture was reduced from 276 to 22 μm, corresponding to a transmissivity reduction of 1.71×10^{-5} to 8.75×10^{-9} m^2/s, over a period of 12 days under constantly flowing conditions. With a modified injection strategy a similar three orders of magnitude reduction in transmissivity was achieved over a period of 3 days. Calcium carbonate precipitated over the entire artificial fracture with strong adhesion to both upper and lower surfaces and precipitation was controlled to prevent clogging of the injection well by manipulating the injection fluid velocity. These experiments demonstrate that microbially induced carbonate precipitation can successfully be used to grout a fracture under constantly flowing conditions and may be a viable alternative to cement based grouts when a high level of hydraulic sealing is required and chemical grouts when a more durable grout is required.

1. Introduction

Rock fracture grouting can be used to both increase the strength of the rock mass and to decrease groundwater ingress into tunnels and other underground engineering works. Traditionally cement based grouts have been used for this purpose; however alternative grouts with the properties of low viscosity and particle size are increasingly being employed. These alternative grouts can penetrate narrow aperture fractures without the need for high injection pressures and can be used near-surface without causing ground heave. Chemical based alternative grouts can be toxic, are typically more expensive in terms of material costs [*Gallagher et al.*, 2013] and have a design life limited to a few decades [*Woodward*, 2005].

A novel alternative grout that offers the potential for sealing small aperture fractures with the mineral calcium carbonate is microbially induced carbonate precipitation (MICP). This process utilizes three components: a ureolytically active bacteria (*Sporosarcina pasteurii*), a calcium source (calcium chloride) and urea which, when hydrolyzed by the urease enzyme, provides the carbon component of the calcium carbonate and increases the pH facilitating the rapid precipitation of calcium carbonate [*Ferris et al.*, 2003]. The MICP process has been investigated for improving strength and stiffness of porous media while maintaining permeability [*Whiffin et al.*, 2007; *van Paassen*, 2009; *DeJong et al.*, 2010a]; permeability reduction in porous media [*Tobler et al.*, 2012; *Handley-Sidhu et al.*, 2013; *Mitchell et al.*, 2013]; immobilizing pollutants [*Mitchell and Ferris*, 2005; *Fujita et al.*, 2008], producing self-healing concrete [*Jonkers et al.*, 2010], and for geological sequestration of CO_2 [*Mitchell et al.*, 2010; *Cunningham et al.*, 2014; *Phillips et al.*, 2016] to name a few.

The use of MICP for grouting rock fractures has been little studied to date. Using individual artificial fractures 20 cm in length, *El Mountassir et al.* [2014] investigated the influence of hydrodynamics on the spatial distribution of $CaCO_3$ precipitated using MICP under a constant flow rate. Their results demonstrate a feedback mechanism between velocity and the development of stable channel-like structures within the $CaCO_3$ precipitate, these channels remained open until flow rates were reduced to enable infilling. *Cunningham et al.* [2009] investigated sealing in a small fracture network (8.5 cm long with 1 mm $\times$ 1 mm diagonal channels

etched into a polycarbonate surface) and found that the flow cell became completely plugged after 20 h but with significant blocking close to the injection point. Few studies have focused on grouting fractured rock at larger scales. *Phillips et al*. [2013] hydraulically fractured and then resealed a 74.3 cm diameter sandstone core under reservoir pressures by stimulating the growth of an *S. pasteurii* biofilm then injecting a single pulse of $CaCl_2$/urea solution, achieving four orders of magnitude reduction in permeability. *Cuthbert et al*. [2013] sealed a natural fracture in dacite, 25 m below ground in a field test of MICP. Fracture sealing effectiveness and $CaCO_3$ distribution were inferred from cross-hole conductance tests between four boreholes. A 99% reduction in transmissivity occurred around the injection well, yet a significant decrease in transmissivity (35%) also occurred at a distance of 2 m from the injection well. However, in both these larger-scale experiments it was not possible to observe the spatial distribution of $CaCO_3$ precipitation and the influence of injection strategy on the resulting precipitation over a large fracture area.

The aims of this paper are to:

1. Identify, in a small-scale artificial fracture, a grout injection strategy that uniformly precipitates calcium carbonate in a controllable manner under continuous flow conditions, and without the formation of channeling within the fracture.
2. Experimentally evaluate the effectiveness of MICP at reducing fracture transmissivity over a large area by sealing an experimental fracture that is close to field-scale.
3. Assess the distribution of $CaCO_3$ precipitation within this fracture and demonstrate control over where precipitation occurs by controlling fluid velocity.
4. To discuss how MICP might be used in practice to grout rock fractures for inhibition of groundwater flow.

2. Experimental Methods and Rationale

2.1. Experimental Setup

A small-scale planar flow fracture composed of a polycarbonate top sheet and a dolerite base was developed for preliminary testing of injection strategies and to study the topography of $CaCO_3$ precipitation with overhead photography and laser scanning (Figure 1). The polycarbonate top sheet enabled visual observation of calcite precipitation within the fracture over time without disturbing the experiment. The flow cell comprised a single fracture (length 394 mm, width 118 mm) with five injection ports and five outlet ports. The fracture aperture was created by embedding a rubber seal into the upper polycarbonate sheet. The

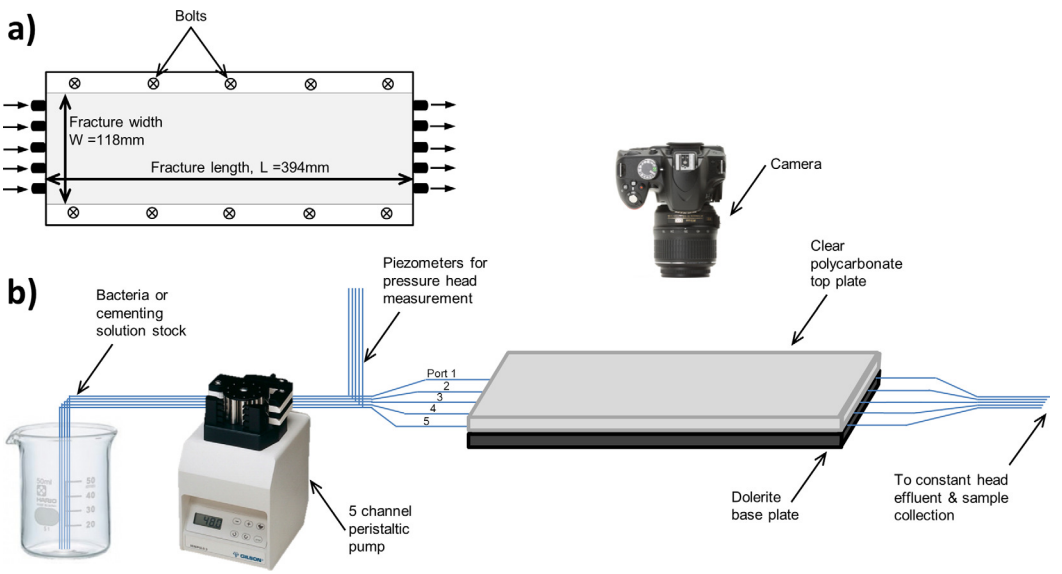

Figure 1. Fracture flow cell (a) plan view and (b) schematic. Fluids injected from a stock reservoir to the fracture by peristaltic pump with five individual injection and effluent lines ensuring uniform flow across the fracture width. Hydraulic head measurements made via piezometers.

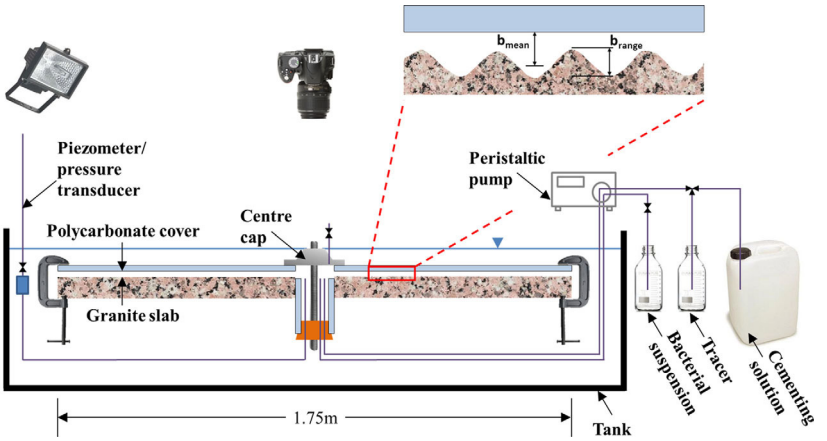

Figure 2. Schematic representation of the large-scale fracture sealing experimental setup and representation of aperture distribution within the artificial fracture.

upper and lower fracture surfaces were then fixed in place via ten bolts, which compressed the rubber seal creating a watertight flow cell with a small fracture aperture. Pressure drop across the fracture flow cell was measured via piezometers at the inlet and by fixing the elevation of the outlet.

Informed by the findings of the small-scale experiment, a large-scale radial flow experiment was developed resembling a borehole intersecting a single planar fracture (Figure 2). The artificial fracture consisted of the interface between a 1.75 m $\times$ 1.75 m saw cut granite slab (unpolished) and a 10 mm thick transparent polycarbonate cover held in place at the center and around the perimeter with clamps. The surface roughness and aperture of the initial artificial fracture differs from a natural fracture due to the saw cut lower granite surface and smooth polycarbonate upper surface. The entire fracture was contained in a water-tight tank and submerged beneath a constant water level (equilibrated to 20°C $\pm$ 1°C in the temperature-controlled laboratory) to maintain a fixed hydrostatic pressure at the fracture outlet. The bacterial suspension, conservative tracer and cementing solution were injected into a central well and thus into the fracture by means of a peristaltic pump. Pressure in the injection well was monitored by piezometer until the pressure exceeded 2 kPa (200 mm H_2O) after which a pressure transducer (sensitive to 0.2 kPa) connected to a data acquisition system (GDS Instruments) recorded well pressure at 30 s intervals. An overhead DSLR camera and lighting system triggered by a microcontroller (Arduino Uno) allowed the collection of a series of high quality images through the polycarbonate fracture cover. In this way, the spatial extent of $CaCO_3$ precipitation based on color change and the transport of a fluorescein tracer were monitored.

2.2. Fracture Aperture and Transmissivity Monitoring

A single injection cycle consisted of first injecting the bacterial suspension followed by a pulse of tap water and then the cementing solution (through a separate injection line), again followed by a pulse of tap water. Multiple injection cycles were undertaken to build up layers of $CaCO_3$ within the fracture and thus progressively reduce the hydraulic aperture. From the well pressure measurements and considering the fixed pressure at the fracture outlets, the hydraulic aperture (b_h) after each injection cycle was calculated using the cubic law for radial flow for the large fracture (equation (1)) and the planar form for the small fracture (equation (2)) [*Witherspoon et al.*, 1980]. Fracture transmissivity (T) was calculated from the hydraulic aperture (equation (3)). Fracture Reynolds number was calculated using an approximation for very long fractures in which the hydraulic diameter is taken to equal twice the fracture aperture (equation (4)) [*Singhal and Gupta*, 2010]:

$$Q_{radial} = \left(\frac{2\pi}{\ln\left(r_0/r_w\right)}\right)\left(\frac{\rho g}{12\mu}\right) {b_h}^3 \Delta h \tag{1}$$

$$Q_{planar} = \frac{w}{L}\left(\frac{\rho g}{12\mu}\right) {b_h}^3 \Delta h \tag{2}$$

$$T = \left(\frac{\rho g}{12\mu}\right) b_h{}^3 \tag{3}$$

$$R_e = \frac{\rho V 2b}{\mu} \tag{4}$$

where Q is the volumetric flow rate at the well [m^3/s], r_w is the radius of the injection well [m], r_0 is the radial distance to a constant hydraulic head boundary [m], L is the planar fracture length [m], ρ is fluid density [kg/m^3], g is acceleration due to gravity [m/s^2], μ is fluid dynamic viscosity [kg/(ms)], Δh is the head loss from injection well to constant hydraulic head boundary [m], V is fluid velocity [m/s], and b is fracture mechanical aperture [m] which is distinct from the hydraulic aperture b_h [m]. As the mechanical aperture of the fractures could not be directly measured with the experimental setups used, hydraulic aperture (calculated with equation (1) or equation (2)) was used as a proxy when calculating Reynolds numbers.

2.3. Bacterial Suspension

Fresh bacterial suspensions were prepared on a daily basis in a procedure similar to that used by *El Mountassir et al*. [2014], *Ferris et al*. [2003], *Mitchell et al*. [2013], and *Tobler et al*. [2014]. Brain heart infusion (BHI) broth (Oxoid) was autoclaved in a Duran bottle then, after cooling, urea dissolved in deionized water and sterilized by passing through a 0.2 μm syringe filter was added to the BHI broth giving a final concentration of 37 g/L BHI, 20 g/L urea. The broth was inoculated with *S. pasteurii* (DSMZ, DSM-33) grown on BHI agar amended with 20 g/L urea. The inoculated broth was then incubated at 28°C on an orbital shaker at 80 rpm for approximately 26 h. Bacteria were harvested by centrifuging at 8000 rpm for six min then resuspended in sterile tap water to the required volume. The bacterial suspension was then injected into the fracture within 2 h of resuspension. Immediately prior to injection, a 1 mL sample was taken for optical density measurement at a fixed wavelength of 600 nm (a measure of the light attenuating properties of the bacterial suspension and hence a surrogate for bacterial cell concentration, hereafter referred to as OD_{600}) and for measurement of the ureolytic activity of the bacterial suspension.

The rate at which *S. pasteurii* can hydrolyze urea is termed the ureolytic activity. It is useful to monitor the ureolytic activity of each bacterial suspension prior to injection to understand the potential for ureolysis and to later make sense of any variation in $CaCO_3$ precipitation and fracture transmissivity reduction. To determine the ureolytic activity of each bacterial suspension, 1 mL of the suspension was added to 9 mL of 1.11 M urea and the change in electroconductivity was monitored over 30 min as nonionic urea was hydrolyzed producing ionic ammonia [*Harkes et al*., 2010]. Provided that there is sufficient urea to prevent the reaction rate being limited, the following equation yields the specific ureolytic activity, i.e., the rate of ureolysis normalized by the optical density of the bacterial suspension:

$$k_{Urea} = \frac{\Delta E.C.}{\Delta t} \frac{C}{\mathrm{OD}_{600} * \mathit{dilution\ factor}} \tag{5}$$

where k_{Urea} is ureolytic activity normalized by OD_{600} [mM urea/min/OD_{600}], $\Delta E.C.$ is the change in electroconductivity between measurements [mS/cm], Δt is the time interval between measurements [min], C the conversion from E.C. change to mM urea hydrolyzed (in this case 10.62 mS/cm = 1 mM urea hydrolyzed), OD_{600} is optical density of original bacterial suspension measured at 600 nm and *dilution factor* = 0.1 to account for dilution when 1 mL of bacterial suspension was added to 9 mL of urea.

2.4. Injection Strategy

When bacteria, $CaCl_2$ and urea are mixed prior to injection, $CaCO_3$ precipitation begins almost immediately in suspension, leading to clogging of the injection ports. Hence, to encourage $CaCO_3$ to precipitate uniformly with strong attachment to the fracture surface, it is necessary to adopt a staged injection strategy, injecting first the bacterial suspension, followed by the $CaCl_2$ and urea cementing solution, but with a small pulse of water in between to prevent mixing and precipitation within the injection lines. This strategy with a rinse step has been successfully employed by *Phillips et al*. [2013] and *Sham et al*. [2013] to minimize plugging of the injection point.

Key to a successful grouting strategy is that the bacteria attach to the fracture surface, otherwise they may be ejected from the fracture without hydrolyzing urea and without contributing to $CaCO_3$ precipitation (e.g., as nucleation sites). To encourage attachment in porous media such as sand, it is common to use a

low concentration (50 mM) $CaCl_2$ solution injected after the bacteria, often termed a "fixer," that promotes bacterial flocculation and attachment by reducing repulsive surface charges [*Whiffin et al*., 2007]. Alternatively a long static period (with or without nutrients for the bacteria) between bacterial and cementing solution injection may be used to encourage attachment [*Cunningham et al*., 2009; *Tobler et al*., 2012]. Natural fractures offer fewer opportunities for mixing than porous media and hence fewer opportunities for a $CaCl_2$ fixer injection to diffuse and overlap with the bacterial injection. Fractures requiring grouting in subsurface engineering works will typically be water-bearing and as such be subject to continuous groundwater flow (i.e., ambient or redirected due to engineering works) preventing the use of a static period for attachment. To overcome this while grouting a natural fracture in the field with MICP, *Cuthbert et al*. [2013] mixed the fixer directly with the bacterial suspension and found sufficient attachment for $CaCO_3$ to precipitate. However, while employing a similar procedure to seal a lab-scale fracture, *El Mountassir et al*. [2014] observed that prior mixing resulted in flocculation of the bacteria before injection, producing large aggregates of $CaCO_3$-coated bacteria, which led to nonuniform precipitation in the form of dendritic-like flow channels within the grouted fracture and poor attachment of $CaCO_3$ to the fracture surfaces. In the experiments presented in this paper, the bacteria were not flocculated and no fixer solution was used.

2.5. Small-Scale Fracture Cell Experiment

The small-scale fracture cell was deployed prior to the borehole-scale experiment to identify an injection strategy that would inhibit the channeling observed by *El Mountassir et al*. [2014] and thus produce a more uniform $CaCO_3$ precipitation under continuous flow conditions. The injection strategy detailed in Table 1 was adopted. Previous MICP experiments in porous media found that biomass clogging alone was capable of reducing permeability [*Nemati et al*., 2005; *Tobler et al*., 2012] due to bacteria cells accumulating in pore throats; in contrast, *Cuthbert et al*. [2013] found that the volume of $CaCO_3$ produced was orders of magnitude greater than the volume of bacteria biomass injected. Hence, for fractures, control experiments without bacteria or with nonureolytic bacteria were not required.

Prior to $CaCO_3$ precipitation, overhead photographs of the fracture surface were taken at 10 s intervals during the injection of a fluorescein tracer to visualize flow paths and to measure tracer travel time.

Laser scans of the lower fracture surface (i.e., dolerite base) were taken using a scanCONTROL 2700 (Micro-Epsilon) scanner before and after precipitation allowing measurement of the initial dolerite surface elevation and the subsequent spatial variation in thickness of the precipitated $CaCO_3$. The scanner procured a series of elevation profiles across the entire fracture width which, when combined, gave fracture surface topography with an *x*,*y* resolution of 200 μm and an elevation resolution of 5 μm.

After dismantling the fracture, laser scanning, and collecting samples for SEM, both top and bottom fracture surfaces were rinsed with tap water. Rinse water was collected, filtered and air dried on a preweighed filter paper to measure mass of $CaCO_3$ washed off. The top and bottom fracture surfaces were then air dried and weighed before all $CaCO_3$ was dissolved with weak (3%) hydrochloric acid. Finally, the top and bottom surfaces were dried and reweighed to calculate the total mass of $CaCO_3$ in the fracture.

Table 1. Small-Scale Fracture Cell Injection Details for a Single Cycle Consisting of Bacteria Injection, Water Pulse to Clear Tubing, Cementing Solution Injection, and Final Water Pulse Before the Following Injection Cycle[a]

Cycle Stage	*Q* (mL/min)	Time	Fracture Volumes (–)	Concentration
Bacteria	1.56	3 h	26	0.5 OD_{600}
Water pulse	1.56	5 min	0.74	
Cementing	1.56	21 h[b]	186	0.7 M urea, 0.5 M $CaCl_2$, pH 6.5
Water pulse	1.56	5 min	0.74	

[a]Fracture volumes is the total volume injected per stage divided by initial fracture liquid volume.
[b]After 3 h of cementing injection the effluent was recirculated to create a closed system that could be left running overnight without a cessation of flow.

2.6. Borehole-Scale Experiments

The injection strategy for the large-scale experiment was based on that employed at the small-scale with the following modifications:

1. Flow is radial, hence velocities are highest at the injection point and approach zero at distance. In order to promote bacterial settling and attachment throughout the fracture surface, the average velocity within the fracture was designed to be equivalent to that in the small-scale planar fracture (0.55 mm/s, see section 3.1). Based on an assumed initial average mechanical fracture aperture of 500 μm, this was achieved with

Table 2. Details of Bacterial Injection Phases for the Large-Scale Experiment[a]

	Cycle	Flow Rate (mL/min)	OD_{600}	Specific Ureolytic Activity (mM urea/min/OD)
Borehole experiment 1 (BHExp1)	*Tracer Prior to First Injection Cycle*			
	1	18.6	0.67	2.47
	2	18.6	0.60	2.65
	3	18.6	0.51	2.61
	Tracer During Third Cementing Cycle			
	4	18.6	0.56	2.85
	5	18.6	0.76	2.68
	6	18.6	0.64	2.31
	Tracer During Sixth Cementing Cycle			
	7	18.6	0.68	1.92
	8	18.6	0.76	1.92
	9	18.6	0.63	2.22
	Tracer During Ninth Cementing Cycle			
	10	9.4	0.81	2.76
	11	9.4	0.88	2.23
	12	9.4	0.54	3.08
	Tracer During 12th Cementing Cycle			
	Average		0.64	2.48
Borehole experiment 2 (BHExp2)	*Tracer Prior to First Injection Cycle*			
	1	19.0	1.19	3.87
	2	19.0	1.09	2.23
	3	19.0	1.30	2.98
	Tracer During Third Cementing Cycle			
	4	19.0	0.65	0.79
	5	19.0	0.60	2.05
	Tracer During Fifth Cementing Cycle			

[a]Specific ureolytic activity is used to compare activity of each bacterial injection.

an injection flow rate of approximately 20 mL/min.

2. The 3 h bacterial injection was retained, necessitating preparation of 4.6 L bacterial suspension (three fracture volumes).

3. Due to the fixed hydrostatic outlet boundary condition, it was not possible to collect the entire effluent for recirculation, yet continuous flowing conditions were still required. Instead, the cementing solution injection volume was increased to 23 L (15 fracture volumes) to allow continuous injection over a 21 h period.

4. The cementing solution was a 0.4 M $CaCl_2$ and 0.4 M urea solution. To prepare 23 L of cementing solution, 1021 g of $CaCl_2$ (MW 110.99) and 553 g of urea (MW 60.06) were added to 20 L of DI water then topped up to 23 L and mixed by overhead stirrer until fully dissolved and equilibrated with the 20°C room temperature. Hydrochloric acid was then added to adjust the pH to 6.5.

5. Bacteria and cementing solution injections were separated by a 0.3 L tap water pulse to reduce mixing of bacteria and cementing solution ensuring that only bacteria that attach to the fractures surfaces contribute to $CaCO_3$ production. This was an important component of the injection strategy and it was envisaged that it would both reduce clogging of the injection point and that the produced $CaCO_3$ would be more strongly attached to a surface rather than crystals produced in suspension and capable of washing out.

Two experiments were conducted at borehole-scale using the large fracture experimental setup; these are termed borehole experiment 1 (BHExp1) and borehole experiment 2 (BHExp2). Table 2 details the flow rate and OD_{600} used during each injection cycle in BHExp1 and BHExp2. In BHExp1, nine cycles were injected at a flow rate of 18.6 mL/min followed by a further three cycles injected at a flow rate of 9.4 mL/min. Due to slight differences in growth time and the amount of bacteria used to inoculate the broth the optical density of the bacterial suspension varied during the 12 injection cycles with an average $OD_{600} = 0.64$. Fluorescein tracer was injected prior to the first injection cycle and toward the end of every third cementing cycle thereafter to visualize the flow paths. In BHExp2, five cycles were injected at a flow rate of 19.0 mL/min and fluorescein tracer was injected before the first, then during the third and fifth cementing cycles. In order to accelerate $CaCO_3$ precipitation relative to BHExp1, in BHExp2 the first three injection cycles used bacterial suspensions with double the OD_{600} (i.e., approximately double the amount of bacteria) while the remaining two cycles had a similar OD_{600} to BHExp1. In BHExp2, the cap covering the injection well was fastened more tightly so as to reduce the aperture at the well; this was done in order to increase the fluid velocity in this region relative to BHExp1.

Based on the injection rate, well radius, and hydraulic aperture, maximum velocities of 3.25 mm/s were predicted to occur adjacent to the well. Using hydraulic aperture in place of mechanical aperture in equation (4) results in Reynolds numbers of 2.0×10^{-6}. Even accounting for variations in mechanical aperture not present when using hydraulic aperture, this is well below the onset of turbulent flow at Re = 100 [*Singhal and Gupta*, 2010] and comfortably within the laminar regime.

By analyzing the images from the time series of overhead photographs, using the image analysis software ImageJ [*Rasband*, 1997–2016], the change in color of each pixel could be measured. Images were first registered (aligned), intensity normalized based on areas outside the fracture surface and then corrected for the

nonuniform background illumination. The intensity was then radially averaged around successive one pixel thick bands extending outward from the injection well to determine how $CaCO_3$ precipitation varies spatially and temporally within the fracture.

3. Experiment Results

3.1. Small-Scale Experiment Results

The results of all injection cycles in the fracture cell are shown in Figure 3. Nine injection cycles of bacteria and cementing solution were completed before terminating the experiment when the hydraulic head at the fracture inlet exceeded 1400 mm H_2O (13.7 kPa) (the maximum height of the piezometers). Initial fracture hydraulic aperture was calculated to be 228 μm. From the tracer transport, the velocity was also estimated giving an average velocity of 0.55 mm/s at the time of tracer breakthrough (Figure 3a). Figure 3b shows images of the $CaCO_3$ precipitation over time at the end of injection cycles 0, 3, 6, and 9. By Cycle 3, $CaCO_3$ precipitation is clearly visible over the entire fracture surface. Until Cycle 6, the fracture transmissivity reduction due to the $CaCO_3$ precipitation was small (Figure 3c). At the end of Cycle 6, one of the five injection lines blocked with $CaCO_3$ leading to a reduction in the inflow from 1.56 to 1.25 mL/min. A second injection line blocked midway through Cycle 8 (at the end of the bacteria injection) further reducing the flow rate to 0.94 mL/min for Cycle 8 cementing injection and Cycle 9. What is clear from Figure 3c is that the largest reductions in fracture transmissivity occur one whole cycle after the reduction in flow rate. Over the full 9 injection cycles of the experiment fracture transmissivity reduced from 9.65×10^{-6} to 3.72×10^{-8} m^2/s; a 99.6% reduction and the limit of what could be measured with the piezometers.

Following the collection of samples for SEM analysis, $CaCO_3$ attachment to the dolerite base was assessed by first gently, then vigorously, rinsing with tap water. Gentle rinsing removed 1.66 g of the 18.85 g attached to the base (8.8%). Vigorous rinsing with a jet of tap water was unable to remove any additional $CaCO_3$ indicating strong attachment to the dolerite. The final mass of $CaCO_3$ was measured as the weight change upon acid digestion: this resulted in a final total mass of 21.51 g of precipitate, 18.85 g of which was attached to the dolerite base and 2.66 g of which was attached to the polycarbonate upper surface.

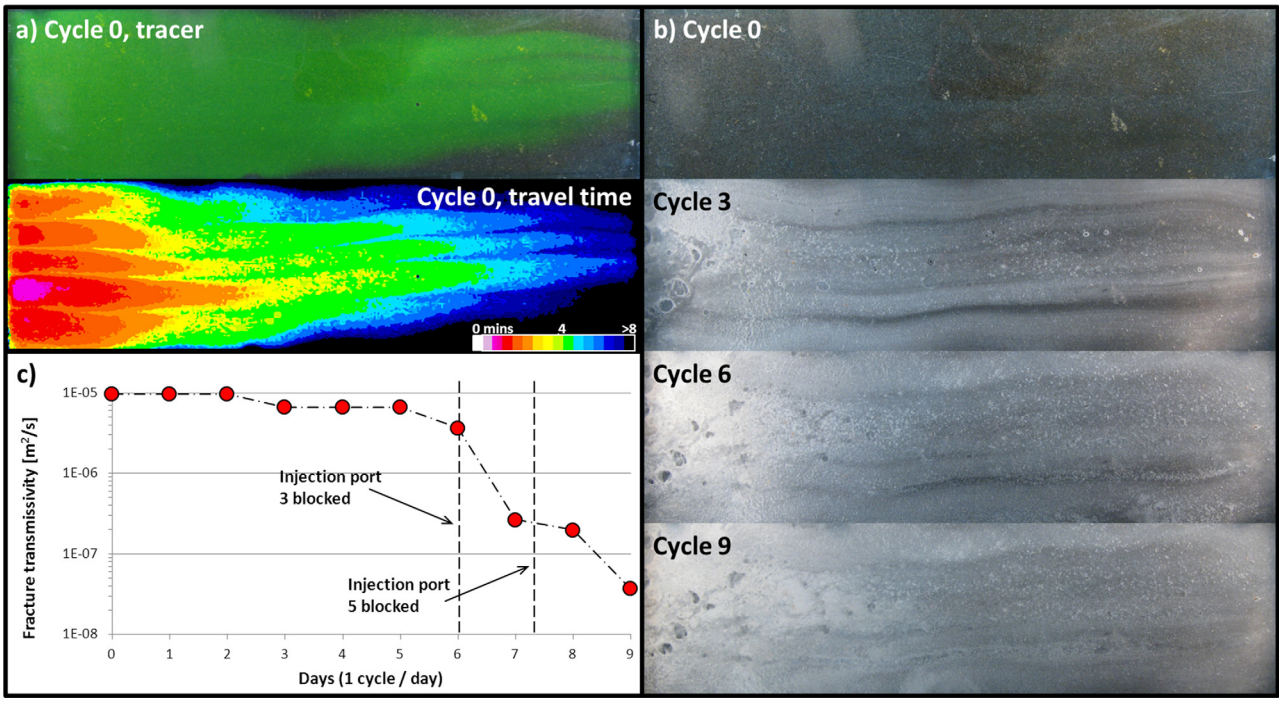

Figure 3. Overhead photographs of the full flow cell surface. (a) Transport of a fluorescent green conservative tracer was photographed at ten second intervals prior to the first injection cycle. Travel time was calculated by analysis of the tracer transport. (b) $CaCO_3$ precipitation clearly visible over the entire fracture surface. (c) Fracture transmissivity was calculated from pressure drop readings taken across the flow plate at the end of each 24 h injection cycle, accounting for reduction in flow rate due to blockage of injection tubing (indicated with vertical dashed lines).

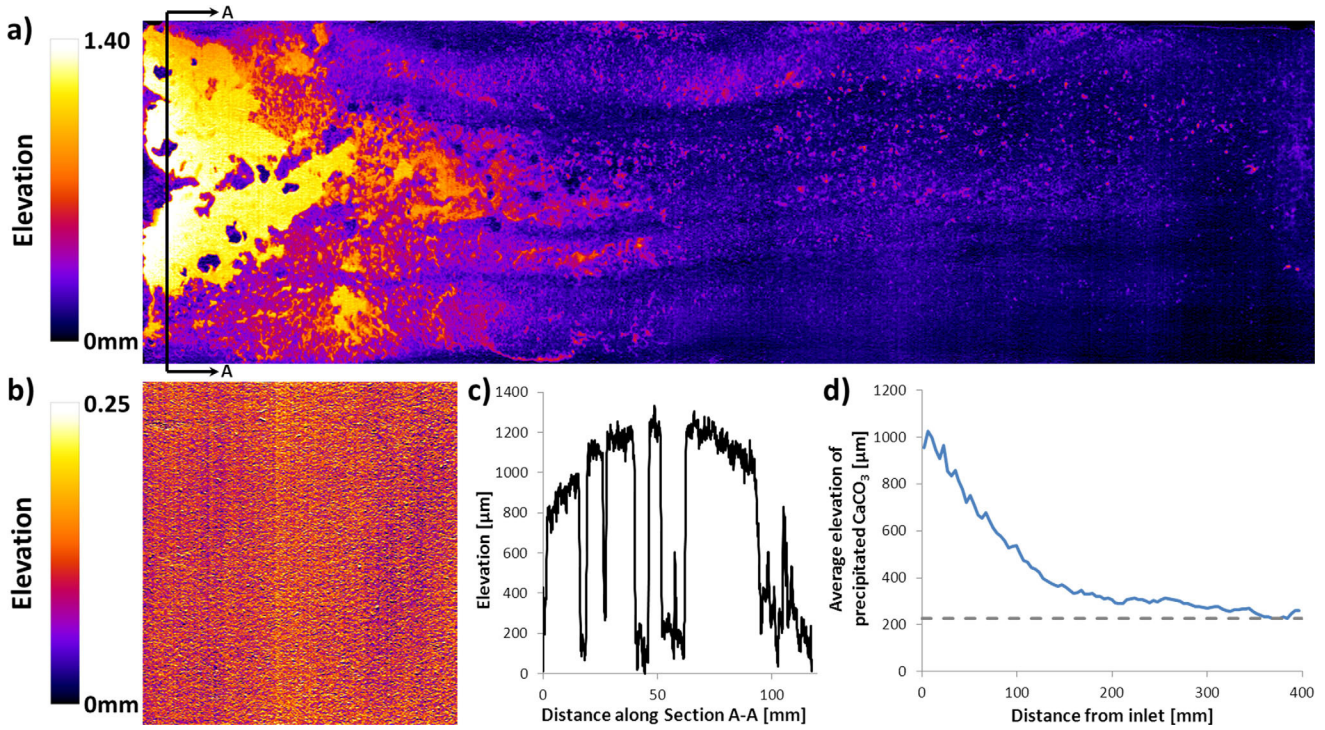

Figure 4. (a) $CaCO_3$ surface elevation relative to the dolerite base, (b) variation in surface elevation prior to $CaCO_3$ precipitation, (c) variation in $CaCO_3$ surface elevation across Section A-A, and (d) average elevation of $CaCO_3$ measured over 4 mm bands from inlet to outlet.

Laser scans of the dolerite base prior to $CaCO_3$ precipitation revealed the surface elevation to be normally distributed with a mean of zero, a standard deviation of 47 μm, and a range of 235 μm over 2.5 standard deviations (encompassing 99% of measurements). After $CaCO_3$ precipitation, the range in surface elevation was 1400 μm, greatly exceeding the calculated initial hydraulic aperture of 228 μm, suggesting that calcite precipitation and crystal growth may have caused bowing of the upper polycarbonate surface. Neglecting void space within the precipitate, the $CaCO_3$ attached to the base, with a density of 2.71 g/cm^3, would occupy 7.9 cm^3 of the fracture volume. The initial fracture volume (based on initial hydraulic aperture) was 10.6 cm^3.

Laser scans of the polycarbonate upper surface could not be made as reflection from, and transmission through, the clear polycarbonate disrupted laser measurement. Hence, the spatial distribution of the mass attached to the upper surface could not be measured (12% of the total $CaCO_3$ precipitated). However, from visual inspection, the polycarbonate appeared to have an almost even coating of $CaCO_3$ over the entire surface.

Figure 4a shows the results of the laser scan at the end of the experiment. For comparison, a section of the initial surface is shown in Figure 4b. Close to the inlet the precipitated $CaCO_3$ had entirely filled the gap between the fracture base and the upper surface. While dismantling the fracture, attachment to the base was greater than to the upper surface resulting in a relatively flat area of $CaCO_3$ with a surface elevation that varies smoothly between 800 and 1400 μm. Section A-A through this flat section (Figure 4c) reveals a domed shape, possibly created by increasing pressure and/or crystal growth deforming the semiflexible polycarbonate during later injection cycles.

The distribution in $CaCO_3$ from inlet to outlet was calculated by dividing the image into a series of bands 4 mm in length and averaged over the entire fracture width. The results (Figure 4d) show greater precipitation within the first 150 mm of the fracture with relatively constant precipitation thereafter.

Overhead photographs of the fracture surface (Figure 3) showed that initially the $CaCO_3$ precipitation followed the flow paths made visible by the Cycle 0 tracer. As $CaCO_3$ was precipitated, these flow paths changed leading to the more even distribution in $CaCO_3$ visible in the laser scan (Figure 4). Despite the

constantly flowing conditions, the formation of stable, open channels observed by *El Mountassir et al.* [2014] in a similar flow cell experiment were absent, presumably as fracture average fluid velocity was considerably lower in the study presented here (0.55 mm/s versus 2–33 mm/s), hence bacterial attachment to the surface was not inhibited.

3.2. BHExp1 Results

Photographs of the fracture taken by the overhead camera prior to the first injection cycle, and after cycles 3, 6, 9, and 12 are presented in Figure 5. Initially the upper polycarbonate fracture surface is transparent and the lower Rosa Porrino granite is pink colored with small black, grey and white areas (Cycle 0). It is evident from Figure 5 that with an increasing number of injection cycles the overhead images become gradually lighter as the fracture becomes progressively filled with white $CaCO_3$.

Analysis of the overhead photographs show the intensity of each pixel increases over time as $CaCO_3$ is progressively precipitated within the fracture; it should be noted here that the relationship between intensity and mass of $CaCO_3$ within the fracture is not linear. From both the photographs and the image intensity analysis it is also apparent that the amount of $CaCO_3$ precipitated is greatest close to the injection well and decreases with distance away from the injection well.

Point measurements of optical density of the fracture effluent (5 mL samples extracted from the midpoint of each of the four fracture sides by syringe) showed no bacterial washout from the fracture during the first injection cycle. Due to the fixed injection rate, as the fracture infills over time with $CaCO_3$, and the fracture aperture reduces, the fluid velocities necessarily increase in the remaining open pathways. This results in

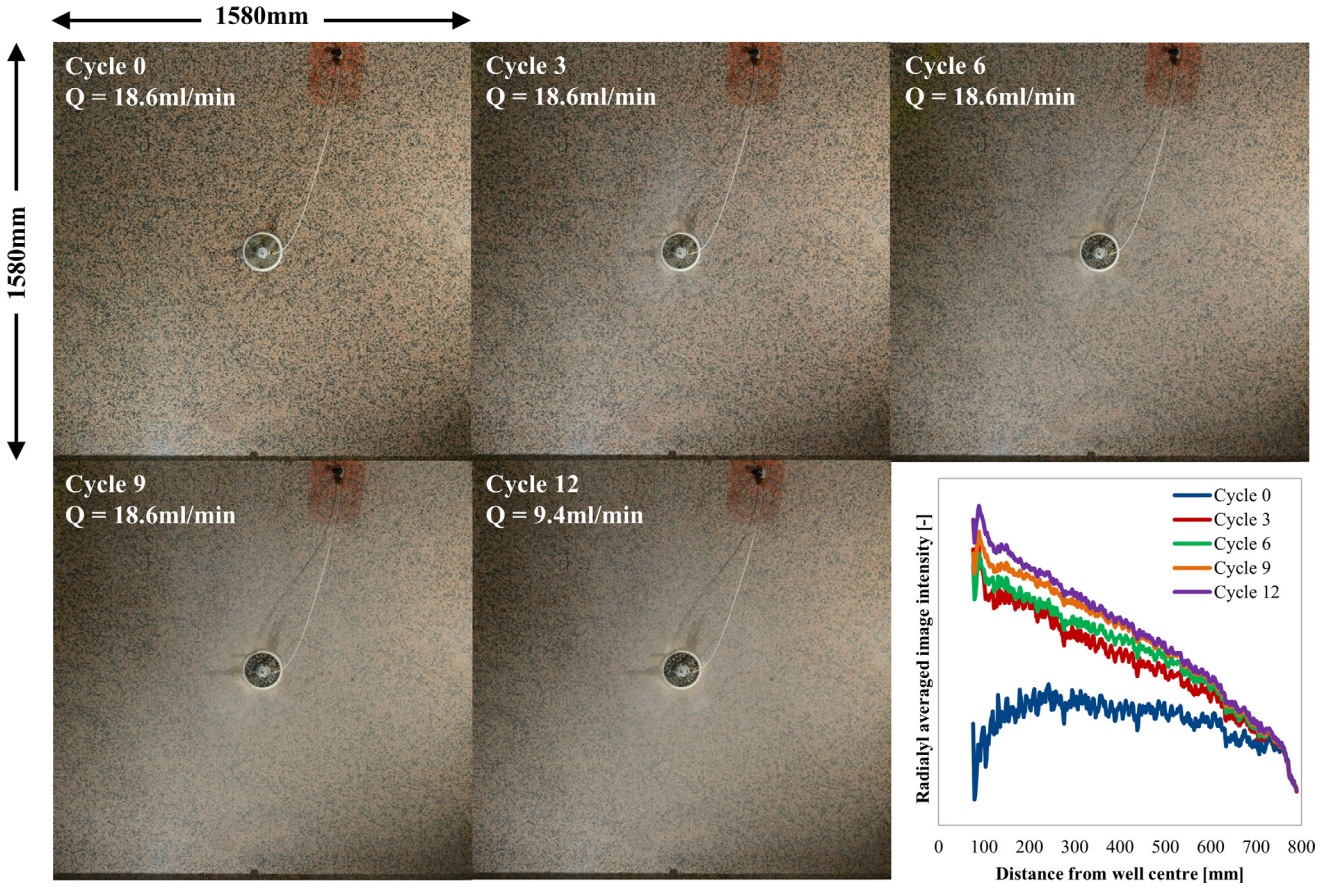

Figure 5. Overhead view of fracture during $CaCO_3$ precipitation. Images are smaller than 1750 mm due to a support frame around the perimeter of the fracture and the shadow this cast. Increase in image intensity (lighter color) was due to $CaCO_3$ precipitation. Amount of precipitation was greatest close to the well, particularly between cycles 9 and 12 when the flow rate was reduced. Plotting the average pixel intensity with radial distance from the injection well center highlighted this trend. N.B. the red spot is paint on the granite surface used by the supplier to identify the stone and does not significantly alter the fracture aperture or bacterial attachment. The tube extending from the injection well is for removing air from the well and is located outside the fracture—above the upper polycarbonate fracture plate.

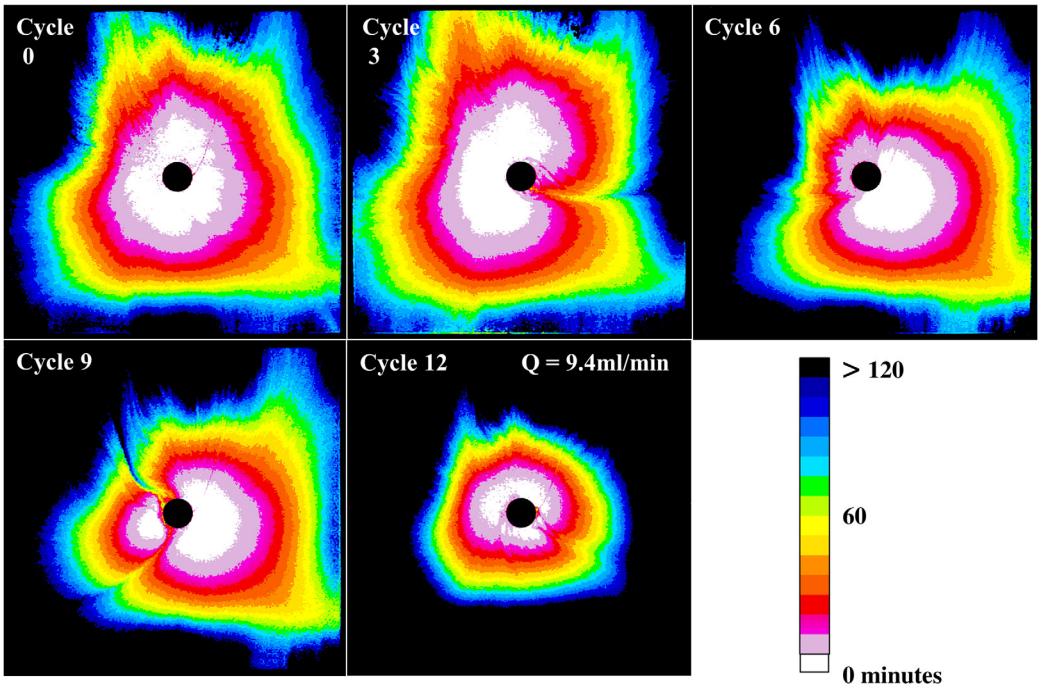

Figure 6. Tracer travel time (i.e., time required for the tracer to be transported from the injection point to each and every point in the fracture) showing change in flow paths as $CaCO_3$ is precipitated. Cycle 0 (top left) is prior to $CaCO_3$ precipitation and represents the baseline flow paths. Note the tracer at cycle 12 was injected at the reduced flow rate of 9.4 mL/min.

bacterial attachment occurring further from the injection well between cycles 3 and 6 (shown in Figure 5) and ultimately, in not all of the injected bacteria being retained within the fracture by cycles 7, 8, and 9. For the final three injection cycles (10, 11, and 12), the injection rate was halved to 9.4 mL/min, reducing the fluid velocity within the fracture. This resulted in an increased amount of $CaCO_3$ precipitated within the vicinity of the injection well and ensured that all bacteria were once again retained.

Flow pathways within the fracture were delineated using a fluorescein tracer. To prevent density dependent flow, the fluorescein was added to the cementing solution and injected at the end of the cementing cycle when the fracture contained cementing solution only. All fluids were given ample time for temperature to equilibrate in the temperature controlled room. Prior to any $CaCO_3$ precipitation, flow paths were approximately uniform within the fracture with travel time increasing radially from the injection well (see cycle 0, Figure 6). Travel time, defined as the time taken between commencement of tracer injection and the tracer front reaching each and every point within the fracture, was determined from time-lapse photography processed with ImageJ.

As $CaCO_3$ precipitated over time within the fracture, the flow paths were altered. In cycle 3, low travel times (indicated by "hot" colors white to orange) were observed in the left hand upper quadrant of the image. However the flow paths in this quadrant had been significantly altered by the end of cycle 6, with very high travel times (black and blue) being observed in this region. In other words, precipitation of $CaCO_3$ during cycles 3–6 has increased travel times in this area by reducing the fracture aperture and shifting the higher flow rates to the bottom right quadrant of the fracture, with a corresponding reduction in travel times in this area. This indicates that there is a positive feedback between flow and $CaCO_3$ precipitation, which is likely due to the increased supply of bacteria and cementing solution in regions of high flow (reduced travel times). During cycles 10–12, the tracer was injected at half of the flow rate used in cycles 1–9, which explains the much higher travel times (in black) over a larger area of the fracture in cycle 12.

Figure 7 shows the evolution of injection pressure with time as precipitation occurs within the fracture. Results show a stepped increase in the injection well pressure recorded with each injection cycle. The majority of the pressure change, and hence the majority of the $CaCO_3$ precipitation, occurred within the first 3 h of the cementing phase of each injection cycle. Movement of the upper polycarbonate fracture surface

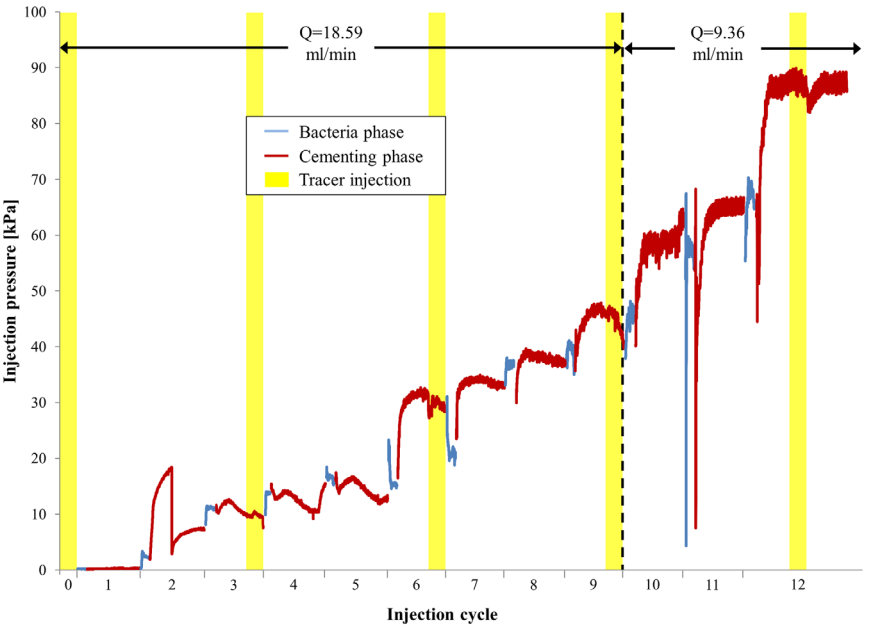

Figure 7. BHExp1 injection well pressure log divided into bacterial injection phase (blue), cementing injection phase (red), and tracer injection (yellow bands). Injections 1–9 were at a flow rate of 18.59 mL/min while 10–12 were at 9.36 mL/min. Each cycle was approximately 24 h long (3.8 h bacteria injection followed by 20.2 h of cementing injection) with the exception of cycle 12 in which the cementing injection time was extended to 40 h.

occurred during cycle 2 when the pressure first reached 19 kPa. After this movement the pressure within the injection well dissipated quickly returning to the pressure recorded at the beginning of the cementing phase in cycle 2. Drops in well pressure occurred in cycle 11 when well pressure reached 69 kPa. Again this was thought to be due to movement of the polycarbonate cover suggesting that 69 kPa is approaching the upper range of injection pressure that can be evaluated with this experimental setup. Figure 5 shows the corresponding reduction in transmissivity over time. Based on the cubic law for radial flow (equation (1)) the initial average hydraulic aperture was 276 μm, which was reduced to 22 μm after 12 injection cycles. This translates to a reduction in average fracture transmissivity from 1.71×10^{-5} to 8.75×10^{-9} m^2/s, a three order-of-magnitude reduction. As shown in Figure 8, the majority of the transmissivity reduction (two orders of magnitude) occurred by the end of the second cycle.

3.3. BHExp2 Results

Based on the results of BHExp1, a second experiment was conducted to determine whether fracture transmissivity reduction could be achieved more rapidly. In the first three cycles of BHExp2, the OD_{600} of the bacterial suspension was double that used in BHExp1 (Table 2). To reduce fracture sealing adjacent to the well itself, the cap at the center of the slab was tightened slightly more than in BHExp1 creating a smaller fracture aperture in the center and hence locally higher velocities for the same injection rate. Figure 9 presents the time series photographs of $CaCO_3$ precipitation within the fracture prior to injection and at the end of cycles 3 and 5. As per the experimental design, in BHExp2 there was visibly less $CaCO_3$ precipitation in the vicinity of the injection well. The image intensity analysis indicates that while some $CaCO_3$ was precipitated close to the well, the highest precipitation rate was at a distance between 400 and 600 mm from the injection well where velocities were between 0.295 and 0.164 mm/s on average. This is in contrast to BHExp1 and the small-scale experiment (both of which were designed to have similar flow velocities), in which the highest rates of $CaCO_3$ precipitation were located close to the injection points. This change in spatial distribution is attributed to reduced bacterial attachment near the well due to the higher velocities resulting from the tightening of the central cap: velocities derived from the tracer transport photographs showed that, within 200 mm of the injection well, the average velocity was 18% higher in BHExp2 than in BHExp1 (Figure 10). It should be noted that the concentration of bacteria attached to the surface is not the only factor contributing to the amount of $CaCO_3$ precipitated; bacterial access to urea, temperature, pH, ionic

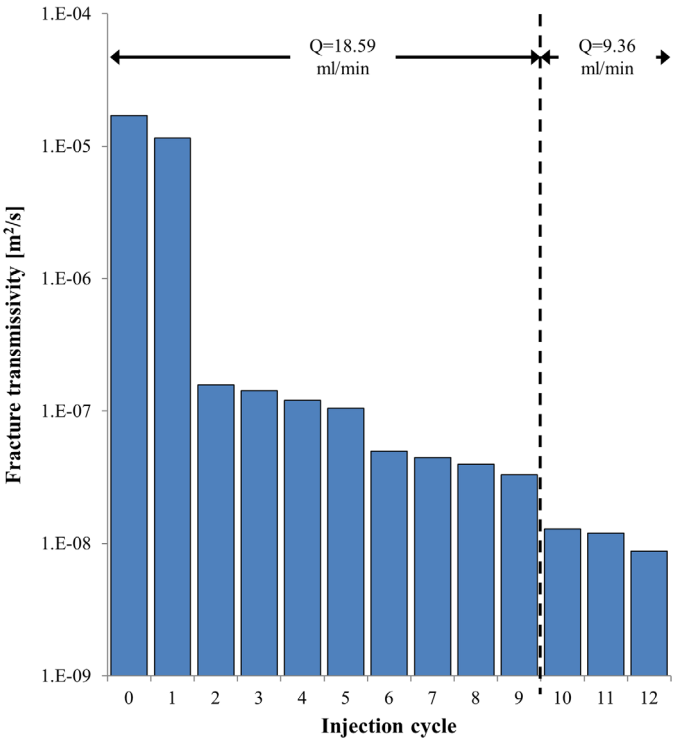

Figure 8. Reduction in calculated fracture transmissivity due to $CaCO_3$ precipitation. A three order of magnitude reduction was achieved with 12 MICP injection cycles, each cycle lasting 24 h.

strength, and dissolved oxygen are also known to influence the ultimate activity of the bacteria [*Stocks-Fischer et al.*, 1999; *Lauchnor et al.*, 2015].

In BHExp2, the hydraulic aperture reduced from an initial value of 334 to 33 μm in five injection cycles. This translates to a three order of magnitude reduction in average fracture transmissivity from 3.05×10^{-5} to 3.10×10^{-8} m^2/s, i.e., similar to that achieved in 12 cycles during BHExp1, with most of the reduction occurring in the first three cycles. As shown in Figure 11, the majority of this transmissivity reduction occurs in the first three injection cycles when bacterial concentration was double that used in cycles 4 and 5 and double that used throughout BHExp1. An increase in transmissivity was observed at the end of cycle 4 which was due to a constriction in the peristaltic pump tubing causing a reduction in the actual flow rate achieved, resulting in an over-prediction of transmissivity. Furthermore cycle 4 had an unusually low specific ureolytic activity compared to that expected for an OD_{600} of 0.65, (see specific ureolytic activity for all cycles in Table 2).

4. Discussion

With the polycarbonate cover of the large-scale fracture removed and the fracture air dried (Figure 12), it was clear from the difference in color that $CaCO_3$ was precipitated extensively in both experiments. As in the small-scale experiment, $CaCO_3$ was precipitated on both the rock and the smooth polycarbonate cover and attachment to both surfaces was so strong that a high pressure water jet was unable to dislodge significant amounts of $CaCO_3$. BHExp1 demonstrated that MICP can be used to build up successive layers of $CaCO_3$ over the entire 3.1 m^2 fracture surface with the effect of reducing fracture transmissivity by three orders of magnitude in 12 injection cycles. BHExp2 showed that the injection strategy can be modified to enable control over where the $CaCO_3$ is precipitated most rapidly by ensuring flow velocities are above a critical threshold and thus limiting bacterial attachment to the surface. BHExp2 also showed that the time taken to grout could be reduced from 12 to three cycles, while still achieving a substantial three order of magnitude reduction in transmissivity. In this respect, the artificial fracture has successfully been grouted with MICP.

4.1. Influence of Injection Rate

In BHExp1, greater $CaCO_3$ precipitation occurred closer to the well and this effect was further enhanced when the injection rate was reduced for the last three cycles. This is in line with filtration theory which can also be (loosely) applied to the transport of the bacteria within the fracture. Slower flow velocities increase the chance that, within a given distance, Brownian motion and sedimentation will bring bacteria close enough to the fracture surface for attachment via van der Waals, electrostatic, acid-base and hydrophobic interaction forces [*Becker et al.*, 2003; *Redman et al.*, 2004; *Tufenkji*, 2007]. In addition, hydrodynamic shear forces which act to prevent attachment are lowered [*Boks et al.*, 2008]. Similar behavior (i.e., increased

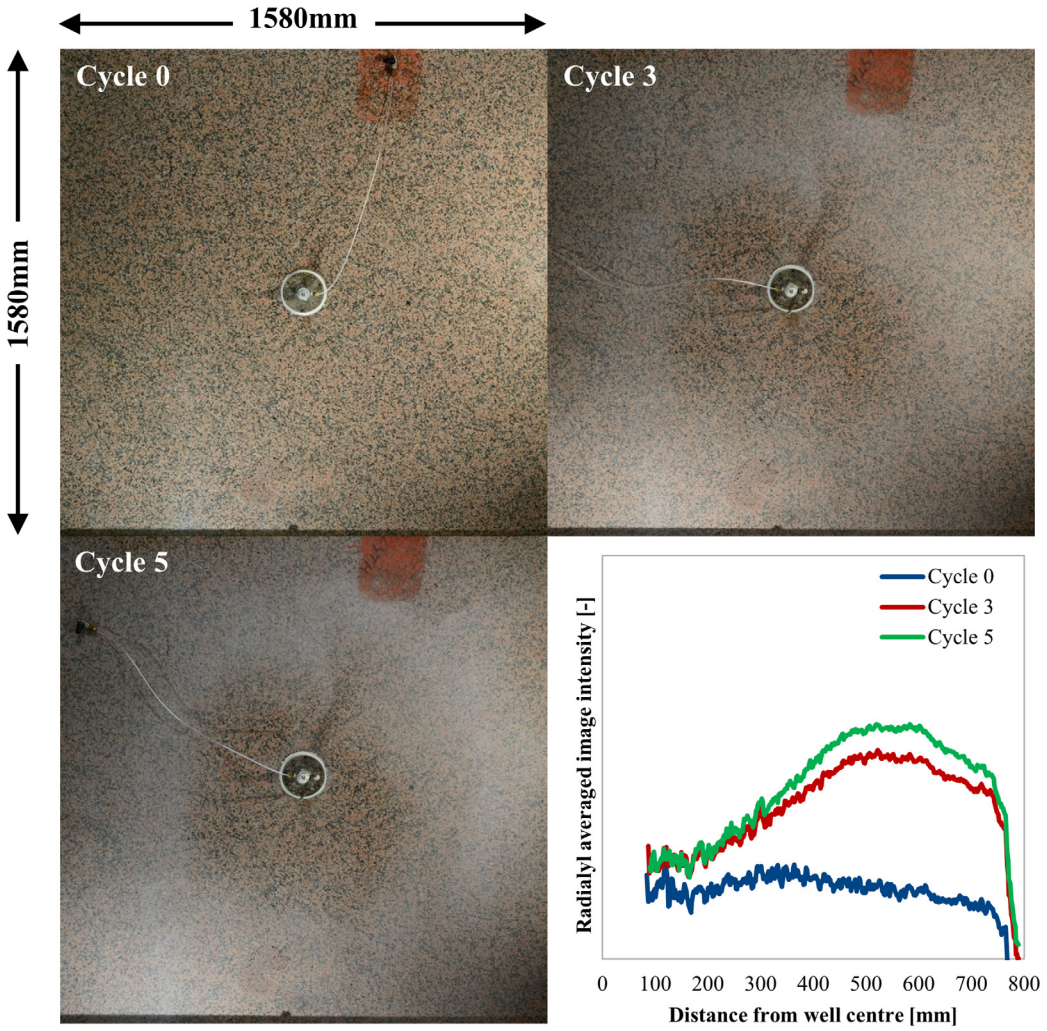

Figure 9. Overhead view of fracture during $CaCO_3$ precipitation. Increase in image intensity (lighter color) was due to $CaCO_3$ precipitation. Amount of precipitation was greatest between 400 and 600 mm from the well with least $CaCO_3$ precipitating in the first 200 mm from the well and at the edge of the granite slab.

bacterial attachment with lower injection rates) of *S. pasteurii* transported through sandstone cores was noted by *Tobler et al*. [2014].

In BHExp2, increasing the velocities close to the well reduced the precipitation rate in the vicinity of the injection well. The highest precipitation rates were observed in a band 400–600 mm from the well, where velocity had decreased sufficiently to facilitate bacterial attachment. In practice, higher velocities close to the well could be achieved by increasing the injection rate up to a limit set only by the necessity to keep pressure below a value which might cause the formation of new fractures. Due to the low viscosity nature of the injection fluids, this limit is unlikely to be encountered in practice until sealing is well advanced as, for example, the maximum injection pressure required in these experiments was 90 kPa. These observations show that varying the injection rate will be a key parameter for design of a grouting strategy.

4.2. Influence of Bacterial Concentration

Increasing the OD_{600} of the first three injection cycles of BHExp2 reduced the number of cycles required for a three order of magnitude reduction in transmissivity from 12 cycles in BHExp1 to three cycles in BHExp2, but the initial reduction in transmissivity occurred at a slower rate in BHExp2 (Figures 8 and 11). This may be because BHExp2 had an initially larger hydraulic aperture than BHExp1 (334 μm versus 276 μm), but also because the region within which $CaCO_3$ is precipitating at its highest rate in BHExp2 is at a greater radial

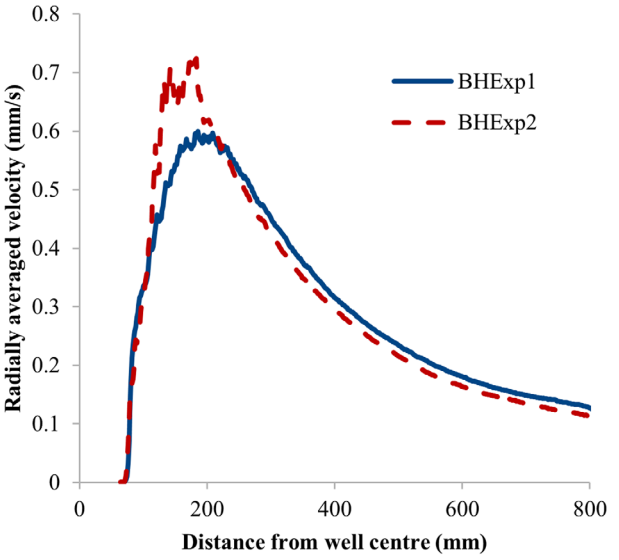

Figure 10. Comparison of BHExp1 and BHExp2 radially averaged flow velocities. Velocities were derived from the time series of tracer transport photographs. Peak velocities were 18% higher in BHExp2 within 200 mm of the injection well due to the reduction in aperture from tightening the well cap. Further from the well, BHExp2 velocities drop below that of BHExp1 due to the larger overall hydraulic aperture of BHExp2 (334 μm versus 276 μm) yet similar injection flow rate.

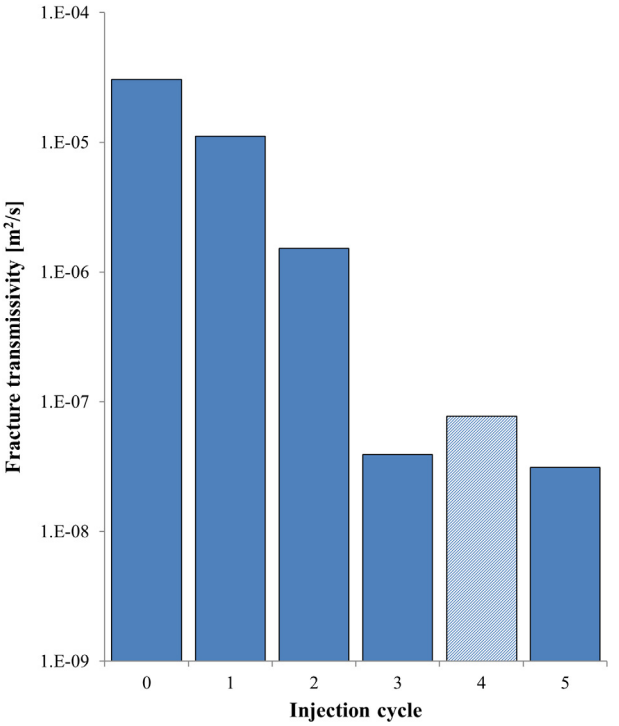

Figure 11. Reduction in calculated fracture transmissivity due to $CaCO_3$ precipitation. A three order-of-magnitude reduction was achieved with three MICP injection cycles. A constriction in the peristaltic pump tubing during cycle 4 is thought to have reduced the flow rate by an unknown amount hence resulting in an over-prediction of transmissivity. Cycle 4 was discounted from further analysis. Each injection cycle lasted 24 h, with the exception of cycle 5 which was terminated 2.5 h into the cementing cycle.

distance from the well and hence covers a larger surface area. As a consequence, the time taken to achieve a similar average hydraulic aperture may be slightly longer.

The majority of the transmissivity reduction of each cycle occurred within the first 3 h of the cementing injection, presumably as bacteria become entombed in $CaCO_3$ [*Stocks-Fischer et al.*, 1999] and effectively become inactive. This suggests that the remaining 17 h of cementing fluid were underutilized. A curtailed cementing fluid injection of 3 h, followed by an injection of fresh bacteria, could reduce both cost and duration of grouting. More work is required to determine optimum concentrations of MICP injection fluids and it should be noted that these may be site specific: in some situations it may be economically preferable to precipitate $CaCO_3$ as rapidly as possible with frequent bacterial injections rather than make the most efficient use of the bacteria and cementing solutions.

4.3. Experimental Limitations

Limitations of this large-scale experiment are its finite size, the requirement for a constant pumping rate, that it is an artificial fracture with no initial filler material, and that a single horizontal fracture was investigated rather than a fracture network. These limitations and their implications for fracture sealing by MICP are discussed further.

Due to the finite size of this experiment, as $CaCO_3$ was precipitated and the fluid velocity within the fracture increased, bacterial attachment decreased, and bacteria were ejected from the fracture. However, if we consider injecting into the subsurface, the bacteria would attach eventually within the wider fracture network and would be available to precipitate $CaCO_3$ at a more distant location from the injection well further decreasing transmissivity. Given the feedback between $CaCO_3$ precipitation and changes to the preferential flow paths observed with the tracers of BHExp1, this would result in more even $CaCO_3$ precipitation over a larger rock volume.

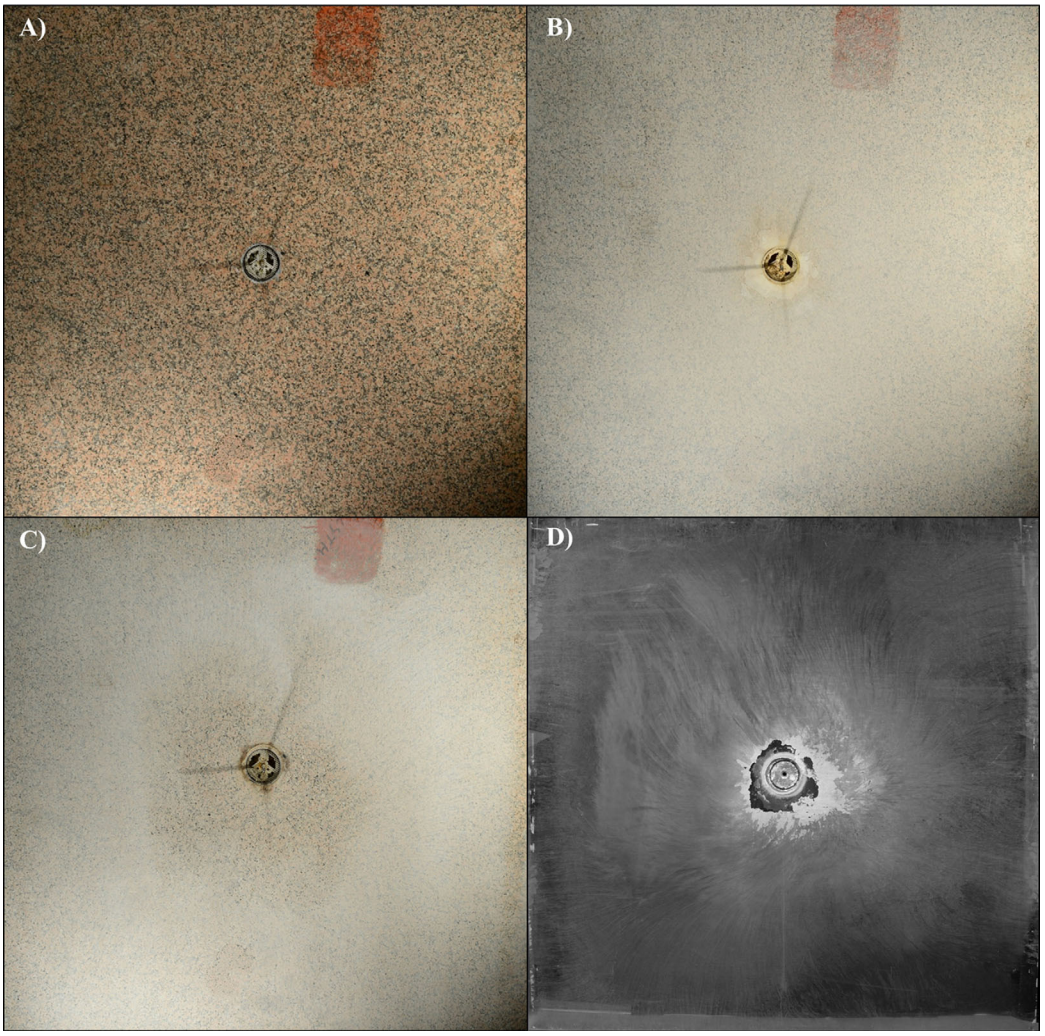

Figure 12. With the polycarbonate cover removed, the granite surface and any $CaCO_3$ precipitated on the lower fracture surface is visible (a) before $CaCO_3$ precipitation, (b) after the 12 injection cycles of BHExp1, and (c) after the five injection cycles of BHExp2. The $CaCO_3$ precipitation on the polycarbonate cover after BHExp1 is visible in Figure 12d i.e., the upper fracture surface matching the lower fracture surface shown in Figure 12b.

As shown in Figure 2, the experimental fracture surfaces differ from natural fracture surfaces in that the lower granite surface was saw cut and the upper surface was polycarbonate. Total $CaCO_3$ precipitation on the upper surface was less than on the lower surface. This is likely due to the upper surface being smooth and only having a bacterial attachment mechanism of electrostatic charge, whereas on the lower surface attachment can be due to electrostatic charge, gravitational settlement, and filtration from surface roughness.

The aperture distribution in the experiment is likely to be more regular than fracture surfaces created by rock shearing, where natural constrictions and fill materials would be present. A less uniform surface and the presence of fill material within the fracture are both more likely to result in more rapid transmissivity reduction, as more surface area is available for bacterial attachment.

The experiments consisted of a single horizontal planar fracture whereas networks of interconnected fractures of different aperture and orientation are likely to be encountered in the subsurface. When it comes to uniformly grouting fracture networks, MICP has an advantage over many other grouts: with a viscosity similar to water and *S. pasteurii* particle size around 4 μm [*DeJong et al.*, 2010b], the MICP injection fluids can penetrate large and fine fractures easily and in most cases the density of the bacterial suspension and cementing fluid can be adjusted to match the groundwater so that density driven flow does not occur. Larger aperture fractures may fill first due to the greater supply of bacteria and cementing fluid but, as was

observed in BHExp1, with each injection cycle the $CaCO_3$ precipitates in layers redirecting flow paths as it does so. In a fracture network, there will come a point when the initially large aperture fractures have been sufficiently sealed such that flow is redirected toward finer fractures. By sealing large and small fractures, the precipitated $CaCO_3$ would form a much more resilient and durable grout than if only the large fractures in the fracture network had been sealed.

4.4. Application of MICP for Fracture Sealing

Through the experiments described above we have shown that MICP is a viable alternative to current technologies for grouting rock with several advantages. The cementation fluid used in MICP is near neutral (adjusted to pH 6.5) and while urea hydrolysis may raise pH closer to 9.3, this is still considered low compared to cement grouts. This makes MICP suitable for construction of radioactive waste geological disposal facilities, where high pH is unacceptable as it interferes with the long-term performance of other safety critical barriers, in particular compacted bentonite. MICP may also be more suitable for construction in environmentally sensitive locations; here the presence of high pH cements could have a negative impact on fragile or valuable ecosystems. However, this must be balanced against the production of ammonium, a by-product of urea hydrolysis that could also harm sensitive environments and may require removal by pumping [*Tobler et al*., 2011] then treatment at a wastewater treatment plant.

Where pH is not an issue, but a high level of hydraulic sealing is desirable, MICP could be applied in combination with an initial phase of cement grouting. As a secondary grout, MICP could be used to seal fine aperture fractures into which microfine cements are unable to penetrate, and to seal shrinkage cracks within the cement-grouted fractures to improve hydraulic performance.

Currently low viscosity grouting is performed using chemical grouts. These provide rapid hydraulic sealing, however, they are often highly toxic and durability is in the order of 10–20 years. In contrast, natural calcium carbonate filled veins and faults have been dated in the 35,000–450,000 year age range [*Flotté et al*., 2001; *Lin et al*., 2003; *Boles et al*., 2004; *Watanabe et al*., 2008] indicating that, unless groundwater is highly acidic, calcite veins can resist dissolution. Further, if tectonic events cause shearing of a calcite filled fracture, the fracture is likely to remain full of calcite crystals, mobile sheared crystal fragments, $CaCO_3$ saturated pore water, and would have a large reactive surface area. Shearing is often accompanied by an increase in temperature (due to friction) and pressure drop (where there is fracture dilation); hence there may be conditions suitable for crystal growth and subsequent grout healing. Our experiments also show that $CaCO_3$ attachment to the fracture surface was very strong, a high-pressure water jet could not remove it, and to clean the fracture for BHExp2 several washes with 3% hydrochloric acid were required. Core-scale experiments are ongoing to determine the shear strength of MICP grouted fractures.

The final advantage of MICP grout is the low injection pressure. The maximum injection pressure reached in these experiments was 90 kPa during the final stages of BHExp1, injection cycle 12, when the fracture hydraulic aperture had reduced to 22 μm. To inject a microfine cement under comparable conditions, assuming a viscosity of approximately 50 mPa s would require an injection pressure of around 3 MPa. Typical maximum grouting pressures are usually in the range of 100–250 kPa per meter overburden, thus precluding the injection of cementitious grouts at depths less than 10–12 m due to the potential for ground heave [*Tolppanen and Syrjänen*, 2003]. By comparison, MICP fluids have a viscosity of, at most, 1.1 mPa s and thus could be used near-surface without risk of uplift.

The main disadvantage of MICP for rock grouting is the time taken to fully grout the rock mass. For some applications, such as geological disposal, tunnels, and shafts are accessible for long time periods and this would not be a major issue. For other infrastructure developments, the advantages of increased durability, improved hydraulic sealing, increased fracture shear strength and reduced environmental impact would need to be weighed up against the additional time required for project completion. As discussed, it may be possible to significantly reduce the grout time by decreasing the duration of the cementation injection stage.

Finally, unlike all other grouts, using MICP the viscosity of the injected fluid does not increase with time; the injected fluid does not begin to set. This opens the door to different injection strategies. For example, it should be possible to grout a far larger rock volume from a single borehole. To achieve this, the initial injection rate would be designed such that the initial fluid velocity was favorable for maximum rates of $CaCO_3$

precipitation at the furthest extent of the design rock volume to be grouted. Injection would then proceed using a constant injection pressure, this would result in a gradual reduction in the flow rate due to fracture sealing at distance and hence in the fluid velocities. As a consequence, precipitation should gradually infill the fracture network from the outside in, i.e., starting at the maximum grouted extent and approaching the injection hole until the entire design rock volume is sealed. Such an approach could significantly reduce the time taken and number of boreholes required for an MICP grouting campaign.

5. Conclusions

MICP is a promising process for sealing rock fractures. We have shown that $CaCO_3$ can be precipitated evenly over a large area, that the rate and location of precipitation can be controlled, and that a significant reduction in fracture transmissivity can be achieved. Due to the low viscosity and low injection pressures, MICP could be applied where use of traditional cementitious grouts is precluded. When a high level of durability, high levels of hydraulic sealing, low pH or minimal injection pressures are desirable, MICP may be a viable secondary grout or even an alternative to current rock grouting techniques.

Acknowledgments
This work was funded by the Engineering and Physical Sciences Research Council (EPSRC) grant (EP/G063699/1), an EPSRC doctoral studentship, and EPSRC Big Pitch grant EP/M016854/1. All experimental data used in this paper are available upon request (email: james.minto@strath.ac.uk).

References

Becker, M. W., D. W. Metge, S. A. Collins, A. M. Shapiro, and R. W. Harvey (2003), Bacterial transport experiments in fractured crystalline bedrock, *Ground Water*, *41*(5), 682–689.

Boks, N. P., W. Norde, H. C. van der Mei, and H. J. Busscher (2008), Forces involved in bacterial adhesion to hydrophilic and hydrophobic surfaces, *Microbiology*, *154*, 3122–3133, doi:10.1099/mic.0.2008/018622-0.

Boles, J. R., P. Eichhubl, G. Garven, and J. Chen (2004), Evolution of a hydrocarbon migration pathway along basin-bounding faults: Evidence from fault cement, *Am. Assoc. Pet. Geol. Bull.*, *88*(7), 947–970, doi:10.1306/02090403040.

Cunningham, A. B., R. Gerlach, L. H. Spangler, and A. C. Mitchell (2009), Microbially enhanced geologic containment of sequestered supercritical CO2, *Energy Procedia*, *1*(1), 3245–3252, doi:10.1016/j.egypro.2009.02.109.

Cunningham, A. B., A. J. Phillips, E. Troyer, E. Lauchnor, R. Hiebert, R. Gerlach, and L. Spangler (2014), Wellbore leakage mitigation using engineered biomineralization, *Energy Procedia*, *63*, 4612–4619, doi:10.1016/j.egypro.2014.11.494.

Cuthbert, M. O., L. A. McMillan, S. Handley-Sidhu, M. S. Riley, D. J. Tobler, and V. R. Phoenix (2013), A field and modeling study of fractured rock permeability reduction using microbially induced calcite precipitation, *Environ. Sci. Technol.*, *47*(23), 13,637–13,643, doi:10.1021/es402601g.

DeJong, J. T., B. M. Mortensen, B. C. Martinez, and D. C. Nelson (2010a), Bio-mediated soil improvement, *Ecol. Eng.*, *36*(2), 197–210, doi:10.1016/j.ecoleng.2008.12.029.

DeJong, J. T., K. Soga, S. A. Banwart, W. R. Whalley, T. R. Ginn, D. C. Nelson, B. M. Mortensen, B. C. Martinez, and T. Barkouki (2010b), Soil engineering in vivo: Harnessing natural biogeochemical systems for sustainable, multi-functional engineering solutions, *J. R. Soc. Interface*, *8*(54), 1–15, doi:10.1098/rsif.2010.0270.

El Mountassir, G., R. J. Lunn, H. Moir, and E. MacLachlan (2014), Hydrodynamic coupling in microbially mediated fracture mineralization: Formation of self-organized groundwater flow channels, *Water Resour. Res.*, *50*, 1–16, doi:10.1002/2013WR013578.

Ferris, F. G., V. R. Phoenix, Y. Fujita, and R. W. Smith (2003), Kinetics of calcite precipitation induced by ureolytic bacteria at 10 to 20°C in artificial groundwater, *Geochem. Cosmochim. Acta*, *67*(8), doi:10.1016/S0016-7037(00)00503-9.

Flotté, N., V. Plagnes, D. Sorel, and A. Benedicto (2001), Attempt to date Pleistocene normal faults of the Corinth-Patras Rift (Greece) by U/Th method, and tectonic implications, *Geophys. Res. Lett.*, *28*(19), 3769–3772.

Fujita, Y., J. L. Taylor, T. L. T. Gresham, M. E. Delwiche, F. S. Colwell, T. L. McLing, L. M. Petzke, and R. W. Smith (2008), Stimulation of microbial urea hydrolysis in groundwater to enhance calcite precipitation, *Environ. Sci. Technol.*, *42*(8), 3025–3032, doi:10.1021/es702643g.

Gallagher, P. M., S. Spatari, and J. Cucura (2013), Hybrid life cycle assessment comparison of colloidal silica and cement grouted soil barrier remediation technologies, *J. Hazard. Mater.*, *250 251–*, 421–430, doi:10.1016/j.jhazmat.2013.01.065.

Handley-Sidhu, S., E. Sham, M. O. Cuthbert, S. Nougarol, M. Mantle, M. L. Johns, L. E. Macaskie, and J. C. Renshaw (2013), Kinetics of urease mediated calcite precipitation and permeability reduction of porous media evidenced by magnetic resonance imaging, *Int. J. Environ. Sci. Technol.*, *10*(5), 881–890, doi:10.1007/s13762-013-0241-0.

Harkes, M. P., L. A. van Paassen, J. L. Booster, V. S. Whiffin, and M. C. M. van Loosdrecht (2010), Fixation and distribution of bacterial activity in sand to induce carbonate precipitation for ground reinforcement, *Ecol. Eng.*, *36*(2), 112–117, doi:10.1016/j.ecoleng.2009.01.004.

Jonkers, H. M., A. Thijssen, G. Muyzer, O. Copuroglu, and E. Schlangen (2010), Application of bacteria as self-healing agent for the development of sustainable concrete, *Ecol. Eng.*, *36*(2), 230–235, doi:10.1016/j.ecoleng.2008.12.036.

Lauchnor, E., D. M. Topp, A. E. Parker, and R. Gerlach (2015), Whole cell kinetics of ureolysis by *Sporosarcina pasteurii*, *J. Appl. Microbiol.*, *118*(6), 1321–1332, doi:10.1111/jam.12804.

Lin, A., N. Tanaka, S. Uda, and M. Satish-Kumar (2003), Repeated coseismic infiltration of meteoric and seawater into deep fault zones: A case study of the Nojima fault zone, Japan, *Chem. Geol.*, *202*(1–2), 139–153, doi:10.1016/S0009-2541(03)00262-6.

Mitchell, A. C., and F. G. Ferris (2005), The coprecipitation of Sr into calcite precipitates induced by bacterial ureolysis in artificial groundwater: Temperature and kinetic dependence, *Geochim. Cosmochim. Acta*, *69*(17), 4199–4210, doi:10.1016/j.gca.2005.03.014.

Mitchell, A. C., K. Dideriksen, L. H. Spangler, A. B. Cunningham, and R. Gerlach (2010), Microbially enhanced carbon capture and storage by mineral-trapping and solubility-trapping, *Environ. Sci. Technol.*, *44*(13), 5270–5276.

Mitchell, A. C., A. J. Phillips, L. N. Schultz, S. L. Parks, L. H. Spangler, A. B. Cunningham, and R. Gerlach (2013), Microbial $CaCO_3$ mineral formation and stability in an experimentally simulated high pressure saline aquifer with supercritical CO^2, *Int. J. Greenhouse Gas Control*, *15*, 86–96, doi:10.1016/j.ijggc.2013.02.001.

Nemati, M., E. A. Greene, and G. Voordouw (2005), Permeability profile modification using bacterially formed calcium carbonate: Comparison with enzymic option, *Process Biochem.*, *40*(2), 925–933, doi:10.1016/j.procbio.2004.02.019.

Phillips, A. J., E. Lauchnor, J. J. Eldring, R. Esposito, A. C. Mitchell, R. Gerlach, A. B. Cunningham, and L. H. Spangler (2013), Potential CO_2 leakage reduction through biofilm-induced calcium carbonate precipitation, *Environ. Sci. Technol.*, *47*(1), 142–149, doi:10.1021/es301294q.

Phillips, A. J., et al. (2016), Fracture sealing with microbially-induced calcium carbonate precipitation: A field study, *Environ. Sci. Technol.*, *50*(7), 4111–4117, doi:10.1021/acs.est.5b05559.

Rasband, W. S. (1997−2016), *ImageJ*, U.S. Natl. Inst. of Health, Bethesda, Md.

Redman, J. A., S. L. Walker, and M. Elimelech (2004), Bacterial adhesion and transport in porous media: Role of the secondary energy minimum, *Environ. Sci. Technol.*, *38*(6), 1777–1785, doi:10.1021/es0348871.

Sham, E., M. D. Mantle, J. K. Mitchell, D. J. Tobler, V. R. Phoenix, and M. L. Johns (2013), Monitoring bacterially induced calcite precipitation in porous media using magnetic resonance imaging and flow measurements, *J. Contam. Hydrol.*, *152*, 35–43, doi:10.1016/j.jconhyd.2013.06.003.

Singhal, B. B. S., and R. P. Gupta (2010), *Applied Hydrogeology of Fractured Rocks*, 2nd ed., pp. 13–34, Springer, Netherlands, doi:10.1007/978-90-481-8799-7.

Stocks-Fischer, S., J. K. Galinat, and S. S. Bang (1999), Microbiological precipitation of $CaCO_3$, *Soil Biol. Biochem.*, *31*, 1563–1571.

Tobler, D. J., M. O. Cuthbert, R. B. Greswell, M. S. Riley, J. C. Renshaw, S. Handley-Sidhu, and V. R. Phoenix (2011), Comparison of rates of ureolysis between *Sporosarcina pasteurii* and an indigenous groundwater community under conditions required to precipitate large volumes of calcite, *Geochim. Cosmochim. Acta*, *75*(11), 3290–3301, doi:10.1016/j.gca.2011.03.023.

Tobler, D. J., E. Maclachlan, and V. R. Phoenix (2012), Microbially mediated plugging of porous media and the impact of differing injection strategies, *Ecol. Eng.*, *42*, 270–278, doi:10.1016/j.ecoleng.2012.02.027.

Tobler, D. J., M. O. Cuthbert, and V. R. Phoenix (2014), Transport of *Sporosarcina pasteurii* in sandstone and its significance for subsurface engineering technologies, *Appl. Geochem.*, *42*, 38–44, doi:10.1016/j.apgeochem.2014.01.004.

Tolppanen, P., and P. Syrjänen (2003), *Hard Rock Tunnel Grouting Practice in Finland, Sweden, and Norway—Literature study*, Finn. Tunnelling Assoc.

Tufenkji, N. (2007), Modeling microbial transport in porous media: Traditional approaches and recent developments, *Adv. Water Resour.*, *30*(6–7), 1455–1469, doi:10.1016/j.advwatres.2006.05.014.

van Paassen, L. A. (2009), *Biogrout: Ground Improvement by Microbially Induced Carbonate Precipitation*, Delft Univ. of Technol., Delft, Netherlands.

Watanabe, Y., S. Nakai, and A. Lin (2008), Attempt to determine U-Th ages of calcite veins in the Nojima fault zone, Japan, *Geochem. J.*, *42*(6), 507–513, doi:10.2343/geochemj.42.507.

Whiffin, V. S., L. A. van Paassen, and M. P. Harkes (2007), Microbial carbonate precipitation as a soil improvement technique, *Geomicrobiol. J.*, *24*(5), 417–423, doi:10.1080/01490450701436505.

Witherspoon, P. A., J. S. Y. Wang, K. Iwai, and J. E. Gale (1980), Validity of cubic law for fluid flow in a deformable rock fracture, *Water Resour. Res.*, *16*(6), 1016–1024.

Woodward, J. (2005), *An Introduction to Geotechnical Processes*, CRC Press, Boca Raton, Fla.